Chemical Engineering Journal 431 (2022) 133213

Contents lists available at ScienceDirect

Chemical Engineering Journal

journal homepage: www.elsevier.com/locate/cej

Eliminating tetracycline antibiotics matrix via photoactivated sulfate radical-based advanced oxidation process over the immobilized MIL-88A: Batch and continuous experiments

Jia-Sheng Wang [a], Xiao-Hong Yi [a], Xingtao Xu [b], Haodong Ji [c], Amer M. Alanazi [d], Chong-Chen Wang [a,*], Chen Zhao [a], Yusuf Valentino Kaneti [b,e], Peng Wang [a], Wen Liu [c,*], Yusuke Yamauchi [b,e,*]

[a] Beijing Key Laboratory of Functional Materials for Building Structure and Environment Remediation, School of Environment and Energy Engineering, Beijing University of Civil Engineering and Architecture, Beijing, 100044, China
[b] International Center for Materials Nanoarchitectonics (WPI-MANA), National Institute for Materials Science (NIMS), 1-1 Tsukuba, Ibaraki 305-0044, Japan
[c] College of Environmental Sciences and Engineering, Peking University, The Key Laboratory of Water and Sediment Sciences, Ministry of Education, Beijing 100871, PR China
[d] Pharmaceutical Chemistry Department, College of Pharmacy, King Saud University, Riyadh 11451, Saudi Arabia
[e] Australian Institute for Bioengineering and Nanotechnology (AIBN) and School of Chemical Engineering, The University of Queensland, Brisbane, QLD 4072, Australia

ARTICLE INFO

Keywords:
Metal-organic frameworks
Sulfate radical-advanced oxidation process
Tetracycline antibiotics
DFT calculations
Wastewater treatment

ABSTRACT

This work demonstrates the successful immobilization of MIL-88A(Fe) MOF on cotton fibers to fabricate MIL-88A (Fe)/cotton fibers (MC) by an eco-friendly method. The prepared MC is used to activate peroxydisulfate for eliminating multiple tetracycline antibiotics, such as oxytetracycline (OTC), tetracycline (TTC), and chlortetracycline (CTC) in simulated wastewater under UV-light irradiation. The photoactivated sulfate radical-advanced oxidation processes (SR-AOPs) towards the removal of tetracycline antibiotics matrix (initial concentration of 10.0 mg/L) using MC were initially investigated using a batch method. The results reveal that 97.5% OTC, 95.2% TTC, and 100.0% CTC can be degraded in the MC/UV/PDS system in the presence of 2 g/L of MC and 1 mM of PDS. The degradation pathways of OTC, TTC, and CTC were clarified *via* liquid chromatography-mass spectrometry analysis and DFT calculations. The quantitative structure–activity relationship analysis shows that the tetracycline antibiotics are transformed into their corresponding intermediates with lower toxicity within 8.0 min. A self-designed fixed bed reactor, in which the MC was packed into the annular channel, was adopted to test the long-term operation possibility of the MC in the continuous photoactivated SR-AOP system. The findings demonstrate that the whole antibiotics matrix can be removed completely within 22 h. This work is the first to demonstrate the use of MOFs as catalysts for SR-AOP to achieve continuous purification of simulated wastewater. The findings highlight a new possibility for the use of MOFs in large-scale wastewater treatment over.

1. Introduction

As emerging environmental pollutants, antibiotics exert serious threat to public health and ecological sustainability [1] due to their difficult elimination by conventional wastewater treatment processes [2,3]. Long-term exposure to low concentration of antibiotics in the environment may result in endocrine disruption and antibiotic resistance in certain organisms [4,5]. Tetracycline antibiotics, such as tetracycline (TTC), oxytetracycline (OTC), and chlortetracycline (CTC) are widely used in the pharmaceutical industry, livestock, agriculture, and aqua-culture [6]. Due to indiscriminate abuse and excess consumption, large quantities of tetracycline antibiotics have been discharged directly into natural ecosystems in the last few decades, leading to serious water pollution [7]. In addition, traditional wastewater treatment plants (WTP) cannot completely remove these antibiotics. Therefore, new approaches, such as, membrane filtration [8], electrolysis [9], and advanced oxidation processes [10] have been developed to remove antibiotics from wastewater. Among these approaches, sulfate

* Corresponding authors at: Australian Institute for Bioengineering and Nanotechnology (AIBN) and School of Chemical Engineering, The University of Queensland, Brisbane, QLD 4072, Australia (Y. Yamauchi).
E-mail addresses: wangchongchen@bucea.edu.cn (C.-C. Wang), wen.liu@pku.edu.cn (W. Liu), y.yamauchi@uq.edu.au (Y. Yamauchi).

https://doi.org/10.1016/j.cej.2021.133213
Received 7 July 2021; Received in revised form 21 October 2021; Accepted 22 October 2021
Available online 29 October 2021

radical-based advanced oxidation processes (SR-AOPs) have been proven to be efficient for removing various organic contaminants [11], in which various reactive oxidation species (ROS), such as sulfate radicals ($SO_4^{-}\bullet$), hydroxyl radicals (•OH), superoxide radicals ($O_2\bullet$), and singlet oxygen ($^1O_2$) are generated to attack these antibiotics. However, inactivated PDS displays limited oxidizing ability towards pollutants and this has led to extensive development of PDS activation technologies for realizing the strong oxidation potential of PDS [12]. For example, heat, ultraviolet (UV) light, and transition metals are often used to accomplish PDS activation. Compared to other transition metal ions, such as Co and Cu ions, Fe ions are more suitable for large-scale applications due to their lower cost and toxicity [13]. Therefore, the use of Fe ions is particularly preferred [14]. However, SR-AOPs based on homogeneous Fe/PDS system typically suffer from several intrinsic drawbacks. The consumption rate of Fe^{2+} is far beyond its regeneration rate [15], which retards the ROS generation and leads to the massive production of waste iron sludge [16]. Thus, SR-AOPs over heterogeneous Fe-based catalysts have attracted significant attention as they demonstrate a wide working pH range as well as excellent stability, and do not generate iron sludge [14]. Meanwhile, metal–organic frameworks (MOFs) have been widely investigated for wastewater treatment. For instance, Jin *et al.* [17] applied Cu, Co co-doped MIL-101 for the adsorption of tetracycline. The doped metals could significantly improve the adsorption capacity of MIL-101. Zhang and co-workers [18] also demonstrated the successful elimination of tetracycline by Fe-MOF activated SR-AOP. The removal efficiency of tetracycline could reach as high as 100%, implying the superiority of SR-AOP compared to the traditional wastewater treatment process.

In recent years, Fe-MOFs as a class of multifunctional porous catalysts, have attracted intense interest [19]. Fe-MOFs are typically obtained by coordinating Fe ions with organic ligands, endowing them with abundant nanopores, large specific surface area, and good thermal stability [20]. Furthermore, Fe-MOFs formed by oxygen-containing organic ligands and Fe ions exhibit the intrinsic absorption characteristics of visible light due to the formation of inorganic nodes of Fe-O clusters, which have aroused great interest from researchers [21]. In addition, they also show excellent thermal and chemical stability. Moreover, Fe element is widely abundant in the earth's crust, making it cheap, and eco-friendly [22]. Due to these attractive characteristics, Fe-MOFs have shown promise as catalysts for heterogeneous Fenton-like reactions in antibiotics removal due to their strong adsorption properties towards pollutants and abundant active metal sites as catalytic sites [23]. Additionally, Fe-MOFs also exhibit high photocatalytic efficiency in pollutant degradation [24] and water splitting [25]. Recently, Fe-MOFs have been applied to activate persulfate with the assistance of UV or visible-light irradiation [26]. For example, MIL-101(Fe) was used in SR-AOP over tris(2-chloroethyl) phosphate, which was further enhanced by adsorption and photocatalytic activation [27]. MIL-88A, an Fe-MOF with Fe as the metal center and fumaric acid as the organic ligand, is a classic and popular MOF that has been applied in photocatalysis [28], adsorption [29], and advanced oxidation processes (*e.g.*, Fenton-like reaction along with PS activation) [30]. Different from other organic linkers for constructing MOFs, fumaric acid displays low toxicity and cost, leading to the better suitability of MIL-88A for wastewater treatment [21]. To date, MIL-88A(Fe) has been shown to be an efficient catalyst for AOP process. Fenton-like and SR-AOP over MIL-88A(Fe) have been widely studied. For instance, Xia *et al.* synthesized rod-like MIL-88A with high phenol removal efficiency [31]. Our group previously explored a heterojunction formed from 3,4,9,10-pyrenetetracarboxydiimine (PDINH) and MIL-88A(Fe), which showed notable photoactivated SR-AOP ability towards chloroquine phosphate (CQ), a possible treatment for coronavirus disease 2019 (COVID-19) [32]. Our group has also reported a mild and facile method to achieve a high throughput production of MIL-88A(Fe) at room temperature by using deionized water and ethanol as solvents [33].

One of the major challenges associated with the use of Fe-MOFs is the inefficient separation and recovery from the aqueous medium after being utilized in wastewater treatment. To overcome this limitation, the immobilization of a powder catalyst onto a supporting substrate may provide an ideal solution. This immobilization process affords efficient separation and easy recovery of the catalyst, while also preventing agglomeration of the catalyst to achieve a higher catalytic performance [34]. In this work, MIL-88A(Fe) particles are immobilized on cotton fibers *via* an in-situ method to fabricate MIL-88A(Fe)/cotton fibers (MC), which is then used to degrade the matrix of multiple tetracycline antibiotics (oxytetracycline, tetracycline and chlortetracycline) in both batch and continuous experiments. Furthermore, investigation of the degradation pathways and evaluation of the toxicity were carried out. Noticeably, one of the main advantages of this work is the achievement of extraordinary durability and stability of immobilized MIL-88A. Up to now, MIL-88A(Fe) can be produced by hydrothermal/solvothermal [35], ultrasonication [36], and microwave-assisted methods [37], in which toxic solvents, such as N, N-dimethylformamide (DMF) are used during the synthesis process. In particular, the high throughput production of MIL-88A(Fe) cannot be accomplished by the above-stated approaches. To the best of our knowledge, this work is the first study to demonstrate the utilization of MOF as a catalyst to accomplish long-term and large-scale continuous purification of wastewater.

2. Experimental

The used chemicals and reagents along with the characterization instruments are provided in the Electronic Supplementary Information (ESI).

2.1. Preparation of MC

In this work MC was prepared according to our previous work with some modifications [29]. Before use, the commercially available cotton fibers were washed several times with ethanol (99%). Next, 400.0 mmol (46.4 g) of fumaric acid and 400.0 mmol (108.1 g) of $FeCl_3{\cdot}6H_2O$ were dissolved in 1.5 L of ethanol (99%) and 1.5 L of deionized water, respectively. Following this, 20.0 g of washed cotton fibers was added into this mixture solution, and subsequently stirred for 48 h with a speed of 80 rpm at room temperature. The obtained MC was washed with deionized water and ethanol (99%) to remove unreacted reagents. The synthetic process was repeated 10 times to ensure the amount of immobilized MIL-88A(Fe) on cotton fibers reached 34.0 ± 1.0 mg per 1.0 g cotton fibers. For comparison, MIL-88A(Fe) powder was synthesized by following the above-mentioned method without the addition of cotton fibers.

2.2. Batch experiment

The performance of MC for photoactivated SR-AOP was investigated under 5 W LED UV light (Beijing Perfectlight Co. Ltd., PCX-50B, wavelength at 369 nm, as illustrated in Fig. S1) (UV-LED). Typically, 0.1 g of the as-prepared MC was added to a 50.0 mL of tetracycline antibiotics matrix of oxytetracycline (OTC), tetracycline (TTC) and chlortetracycline (CTC), each with initial concentration of 10.0 mg/L) in a quartz reactor, followed by the addition of 50 μL of 1000 mmol/L sodium peroxydisulfate (PDS) solution. At a fixed time-interval, 0.3 mL of the suspension was taken out and filtered *via* a 0.22 μm syringe filter for subsequent determination. The residual concentrations of tetracycline antibiotics were determined by Vanquish Duo high performance liquid chromatograph (HPLC) equipped with a C18 column (2.1 mm × 250 mm, 5.0 μm). The detection wavelength of the UV detector was set as 355 nm. Moreover, KCl, $CaCl_2$, $MgCl_2$, Na_2SO_4, $NaNO_3$, and NaH_2PO_4 were introduced into the aqueous solution containing tetracycline antibiotics matrix to simulate the exact concentrations of inorganic cations (*e.g.*, K^+, Ca^{2+} and Mg^{2+}) and anions (*e.g.*, Cl^-, NO_3^-, SO_4^{2-} and $H_2PO_4^-$ in real groundwater, like Cl^- = 135.3 mg/L, NO_3^- = 13.6 mg/L, SO_4^{2-}

= 124.0 mg/L, $H_2PO_4^-$ = 5 mg/L, K^+ = 4.68 mg/L, Ca^{2+} = 185 mg/L, Mg^{2+} = 39.7 mg/L [32,38]. Additionally, the unadjusted initial pH value of the tetracycline antibiotics matrix was 4.04. In the active species capture experiments, methanol (MeOH), tertiary butyl alcohol (TBA), L-histidine, and EDTA-2Na were selected as active species quenchers. The concentration of each quencher was 30 mM. Noticeably, a simulated wastewater containing OTC, TTC and CTC with initial individual concentration of 10.0 mg/L was selected to clarify the degradation pathway of individual tetracycline antibiotics in photoactivated SR-AOP.

2.3. Fixed bed reactor experiment

In a typical process, 6.204 g of the as-prepared MC was inserted into a self-designed annular quartz equipment with a reaction volume of 120.0 mL to construct the fixed bed reactor, in which a 10 W high pressure mercury UV light (UV-Hg) with wavelength of 256 nm (CNlight) was placed in the central cavity to provide light irradiation (Scheme 1). The simulated wastewater containing tetracycline antibiotics (TTC, OTC and CTC), each with initial concentration of 10 mg/L) matrix was pumped into the fixed bed reactor by peristaltic pump with a flow rate of 0.2 L/h, in which the PDS solution (1 mol/L) was injected using a high-precision injection pump with a flow rate of 300 μL/h.

3. Results and discussion

3.1. Synthesis and characterizations

In this work, a simple and green approach is developed to immobilize MIL-88A(Fe) on cotton fibers without heating process and the use of toxic solvents. It is worth to noting that this approach can achieve large-scale and in-situ production of MC without the need for any separation process, such as centrifugation or filtration. Therefore, our method is superior to other production strategies reported previously.

The 2θ peaks at 8.0°, 10.5°, 13.3°, and 15.7° in the powder X-ray diffraction (PXRD) pattern of the as-prepared MIL-88A(Fe) powder (Fig. S2) match well with the standard PXRD patterns of MIL-88A(Fe) (Fig. S3) and previously reported MIL-88A(Fe) [29,39], thus confirming the successful synthesis of MIL-88A(Fe). The formation of MIL-88A (Fe) was further confirmed by scanning electron microscopy (SEM), Fourier transform infrared (FTIR) spectroscopy, and X-ray photoelectron spectroscopy (XPS). However, due to the small content of MIL-88A in MC (34 ± 1.0 mg MIL-88A on 1.0 g cotton fibers), only the characteristic peak at 10.5° of MIL-88A (Fig. S2) is observed in the PXRD pattern of MC [29]. Well-crystallized hexagonal MIL-88A rods with lengths of 300–400 nm and diameters of 100–200 nm are uniformly immobilized on the cotton fibers (Fig. 1), which are significantly smaller than previously reported MIL-88A particles [33,37,40].

The presence of MIL-88A in MC was further confirmed by UV–vis spectroscopy (Fig. S4), FTIR (Fig. S5), and XPS (Fig. S6), and the corresponding results and discussion are discussed in ESI. The existence of C−O−C peak (288.78 eV) in the C 1*s* XPS spectrum of MC and the −COOR band (at 1734 cm^{-1}) observed in the FTIR spectrum of MC confirm the presence of ester group. The esterification takes place between the carboxylate from fumaric acid and hydroxyl from cellulose [29]. Compared to the unsupported MIL-88A(Fe) powder, the combination of ligand and cotton fibers enhances the stability of immobilized MIL-88A.

3.2. Photoactivated SR-AOP performance of MC in batch experiment

3.2.1. Tetracycline antibiotics matrix degradation

The photoactivated SR-AOP degradation performance of MC towards tetracycline antibiotics matrix was evaluated in the presence of UV-LED light and PDS and a series of control experiments were also conducted. As shown in Fig. 2, after 8 min of irradiation under UV-LED light, the self-degradation efficiencies of OTC, TTC, and CTC in the matrix are *ca.* 6.9%, 2.7%, and 2.5%, respectively. Only *ca.* 10% OTC, TTC, and CTC are removed in the presence of individual PDS under dark condition. About 30% OTC, TTC, and CTC removal are achieved using MC without

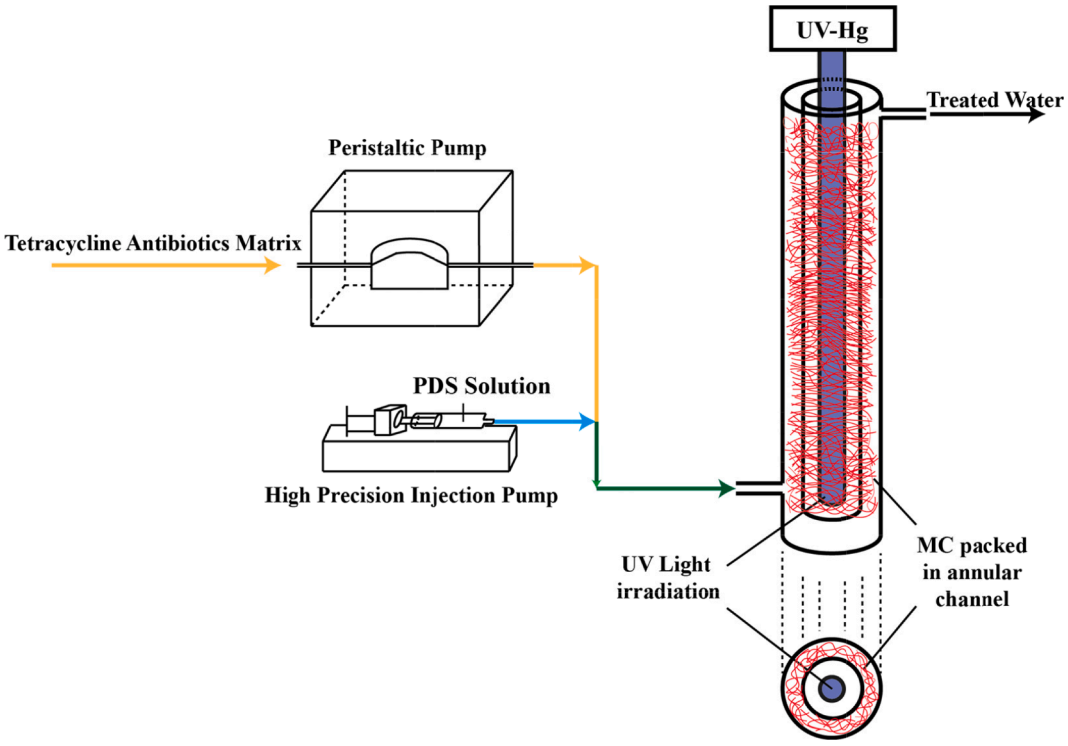

Scheme. 1. Schematic diagram of the fixed bed reactor. Volume of annular channel = 120 mL, flow rate of tetracycline antibiotics matrix = 0.2 L/h, and flow rate of PDS solution = 300 μL/h.

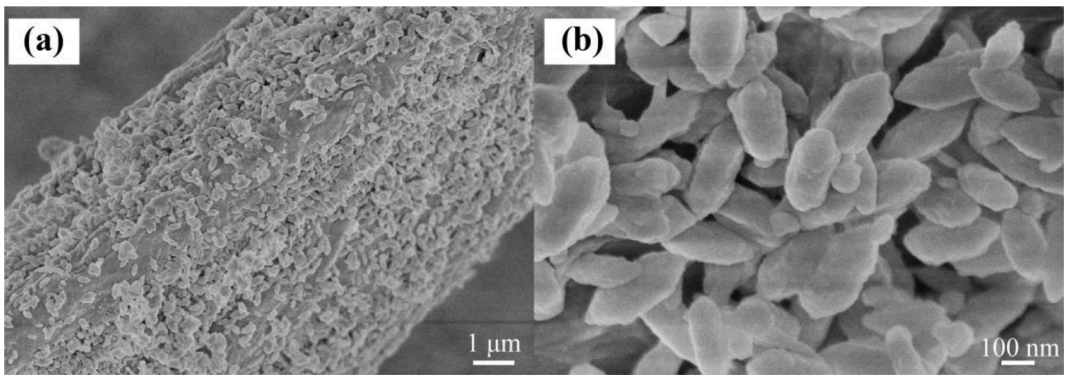

Fig. 1. (a) Low- and (b) high-magnification SEM images of MC.

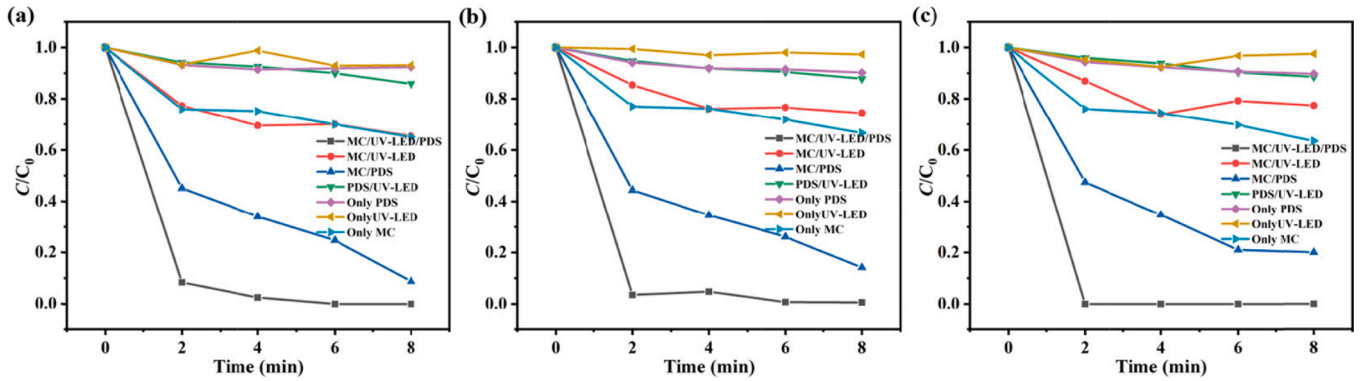

Fig. 2. The tetracycline antibiotics matrix (a: OTC; b: TTC and c: CTC) degradation in different systems. Reaction conditions: MC = 2 g/L, OTC = 10 mg/L, TTC = 10 mg/L, CTC = 10 mg/L, volume = 50.0 mL, PDS = 1 mM, pH = 4.04 (unadjusted), sampling interval = 2 min.

both UV irradiation and the addition of PDS, due to the high adsorption capacity of MIL-88A(Fe). Only *ca.* 15% OTC, TTC and CTC are removed within 8 min with the addition of only PDS into the reaction system under UV-LED light irradiation, suggesting that the photoactivated PDS cannot produce sufficient active species for degradation of organics. When both MC and PDS are added to treated wastewater containing OTC, TTC, and CTC matrix under UV light, an obvious increase in degradation activity is observed, indicating that more active species are produced to degrade tetracycline antibiotics. The degradation efficiencies of OTC (97.5%), TTC (95.2%), and CTC (100%) in MC/UV-LED/PDS system within 4 min are much higher than those (40.6% for OTC, 23.9% for TTC and 35.4% for CTC) achieved in MC/PDS system, implying that photoactivated SR-AOP plays a predominant role in the degradation of tetracycline antibiotics over MC under UV-LED irradiation. Additionally, total organic carbon (TOC) removal efficiencies of 25.5% and 51.9% can be accomplished within 4 min and 60 min for tetracycline antibiotics matrix, respectively (Fig. S7).

3.2.2. *Effect of initial pH*

In general, it is essential to investigate the effect of pH on the degradation efficiency, as it may influence the surface charge of the catalyst as well as the form of the targeted pollutant. The influence of initial pH on the degradation of tetracycline antibiotics in the matrix was explored by conducting a series of experiments in the pH range of 2.0 to 9.0 (Fig. 3). The results reveal that the decomposition of tetracycline antibiotics in MC/light/PDS system can be achieved over a wide pH range. Lower pH values (2.0–7.0) are beneficial for the degradation of tetracycline antibiotics matrix. More than 99% degradation efficiency

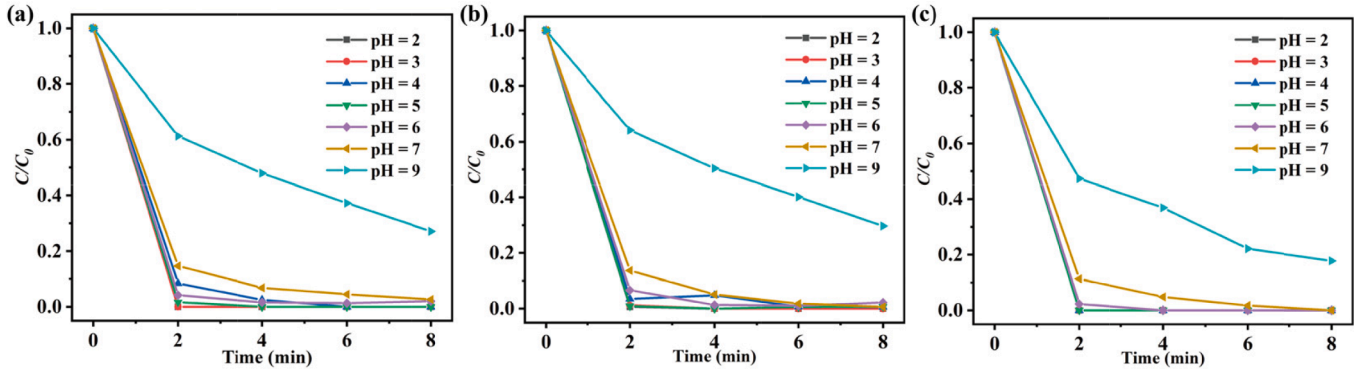

Fig. 3. Effect of initial pH on the degradation of tetracycline antibiotics (a) OTC, (b) TTC, and (c) CTC over MC. Reaction conditions: MC = 2 g/L, OTC = 10 mg/L, OTC = 10 mg/L, TTC = 10 mg/L, CTC = 10 mg/L, volume = 50 mL, PDS = 1 mM, sampling interval = 2 min.

can be accomplished in the pH range of 2.0–7.0 within 10 min. In general, SO_4^{-}• is more likely to be generated under acidic conditions, according to Eqs. (1) and (2). However, SO_4^{-}• can be transformed into SO_4^{2-} and •OH following Eqs. (3) and (4) under alkaline conditions, which decrease the generation of SO_4^{-}• radicals for degradation of pollutants.

In this study, individual adsorption tests between selected antibiotics and immobilized MIL-88A(Fe) under dark condition were not carried out, as all three tetracycline pollutants can be degraded completely within a short time (2–4 min). In our system, the influence of pH towards the adsorptive interactions between selected antibiotics and immobilized MIL-88A(Fe) is rather negligible. Previous studies pointed out that all three tetracycline antibiotics (the pKa_1 values of OTC, TTC, and CTC being 3.23, 3.30 and 3.30, respectively) could form cations under strong acidic conditions [41–43], while MIL-88A(Fe) exhibited a positive zeta potential [29]. Furthermore, under weak acidic and neutral conditions, the three tetracycline antibiotics (pKa_2 = 7.22, 7.70 and 7.44 for OTC, TTC, and CTC, respectively) were in neutral form. Meanwhile, the change in zeta potential of MIL-88A(Fe) from positive to negative is observed under weakly acidic and neutral conditions. Additionally, under alkaline conditions, tetracycline antibiotics are in anionic forms, while MIL-88A(Fe) exhibits negative zeta potentials, suggesting the electrostatic repulsion between MIL-88A(Fe) and tetracycline antibiotics. It is believed that the large pore volume of MIL-88A(Fe) [44] as well as π-π interactions and hydrogen bonding interactions between MIL-88A(Fe) and tetracyclines [45,46] jointly contribute to the accumulation of these three tetracycline antibiotics to the active sites and allow for effective degradation.

It is believed that pH can heavily influence the stability of MIL-88A [33,47]. As a typical MOF constructed from "hard" metal ions (Fe^{3+}) and polycarboxylate ligands (fumaric acid), MIL-88A(Fe) exhibits good stability in acidic solutions [48]. However, MIL-88A(Fe) may collapse in alkaline conditions due to the lower p*K*a of fumaric acid [33]. More importantly, the initial pH of the simulated wastewater containing tetracycline antibiotics matrix is 4.04, allowing for the full utilization of photoactivated SR-AOP performance and water stability of the immobilized MIL-88A(Fe). Therefore, the working pH of this system is maintained at *ca.* 4.04 without further adjustment.

$$S_2O_8^{2-} + H^+ \rightarrow HS_2O_8^- \quad (1)$$

$$HS_2O_8^- + e^- \rightarrow SO_4^{-}\bullet + SO_4^{2-} + H^+ \quad (2)$$

$$SO_4^{-}\bullet + H_2O \rightarrow SO_4^{2-} + \bullet OH + H^+ \quad (3)$$

$$SO_4^{-}\bullet + OH^- \rightarrow \bullet OH + SO_4^{2-} \quad (4)$$

3.2.3. Effect of co-existing inorganic ions

Different ions are usually present in real water environments, which may have negative impact on the advanced oxidation process [18,30] and the stability of MOFs [40,49]. To investigate the practicality of the proposed MC/light/PDS system, the simulated wastewater was prepared by dissolving the tetracycline antibiotics matrix into an aqueous solution containing inorganic ions, including K^+, Ca^{2+}, Mg^{2+}, Cl^-, NO_3^-, SO_4^{2-}, and $H_2PO_4^-$. The concentrations of these ions were adjusted according to a previous report [38].

It has been reported that the degradation of tetracycline antibiotics in aqueous solutions may be inhibited by the co-existence of inorganic metal ions due to the generation of $[Metal\text{-}TC]^+$ [50]. Common cations, such as Ca^{2+}, Mg^{2+}, K^+, Na^+ have been found to exert negligible impact on the SR-AOP [51]. However, inorganic anions, such as $H_2PO_4^-$, Cl^-, SO_4^{2-}, and NO_3^- may act as scavengers to consume the radicals or as reactants to convert the more active radicals to less active ones [52]. Fortunately, the degradation activity of the photoactivated SR-AOP over immobilized MIL-88A(Fe) catalyst is barely affected by the various inorganic anions (Fig. 4), with 100% degradation efficiency towards TTC and CTC as well as >90% efficiency towards OTC being achieved in the presence of other inorganic anions. To further explore the degradation efficiency in real wastewater treatment, aqueous solutions with different cations and anions were used to simulate a wastewater containing tetracycline antibiotics. In the simulated wastewater containing three cations (*i.e.*, K^+, Ca^{2+}, and Mg^{2+}), no obvious decline in the degradation efficiency is observed. As for the simulated wastewater containing four anions (Cl^-, NO_3^-, SO_4^{2-}, and $H_2PO_4^-$), approximately 91%, 95% and 93% of OTC, TTC, and CTC can be removed through the SR-AOP, respectively. It is well known that $H_2PO_4^-$ can act as a potential scavenger for •OH [53]. Meanwhile, SO_4^{2-}, as the extra sulfate, may compete with $S_2O_8^{2-}$, thereby causing the reduction in degradation efficiency [54]. Nonetheless, >90% of OTC, TTC, and CTC can be eliminated in both types of simulated wastewater, implying that the photoactivated SR-AOP using MC/light/PDS system can be potentially used to treat real wastewater containing different organic pollutants. The concentrations of each mentioned inorganic cations and inorganic anions based on surface water in some areas in Beijing are listed in the caption of Fig. 4 [32,38].

3.2.4. Possible degradation mechanism of photoactivated SR-AOP over MC

The active radicals generated in the photoactivated SR-AOP over MC were identified by the active species capture experiments (Fig. 5). Methanol (MeOH) can strongly react with both SO_4^{-}• and •OH radicals with nearly similar reaction rate constants of 1.0×10^7 M^{-1} s^{-1} and 9.7×10^8 M^{-1} s^{-1}, respectively. However, TBA is likely to react with •OH with a faster reaction rate of $(3.8 \sim 7.6) \times 10^8$ M^{-1} s^{-1} than that of SO_4^{-}• ($4.0 \sim 9.1 \times 10^5$ M^{-1} s^{-1}) [55]. When 1 mL of 0.5 mol L^{-1} MeOH is added, the degradation efficiencies of MC towards OTC, TTC, and CTC without any scavenger are significantly decreased from 100% to 33.8%, 26.8%, and 47.4%, respectively, indicating that the SO_4^{-}• and •OH radicals produced in the reaction system are greatly quenched. When 1 mL of 0.5 mol L^{-1} TBA is added, the degradation efficiencies decrease to 64.2%, 66.8%, and 65.2% for OTC, TTC, and CTC, respectively, confirming that a large amount of •OH radicals is generated during the photoactivated SR-AOP. By comparing the quenching effects of MeOH and TBA as radical scavengers in the reaction, the removal efficiencies of all three tetracycline antibiotics are significantly lowered in the presence of MeOH, suggesting that SO_4^{-}• and •OH radicals are the primary and secondary active species in the reaction system [56].

Further, EDTA-2Na and L-histidine can act as scavengers to capture the h^+ and singlet oxygen ($^1O_2$) [32,57]. When EDTA-2Na and L-histidine are introduced into the MC/UV-LED/PDS system, no obvious decrease in degradation efficiencies towards the three tetracycline antibiotics is observed, indicating that h^+ and non-radical $^1O_2$ are not involved in the photoactivated SR-AOP towards tetracycline antibiotics. In addition, the electron spin resonance (ESR) spectrum is shown and discussed in Supporting Information (Fig. S8).

3.2.5. Possible degradation pathways and toxicity assessment

Density functional theory (DFT) calculation of the Fukui index was used to analyze the reactive sites of organic molecules in photoactivated SR-AOP over MC catalyst. In this study, the primary active species are electrophilic radicals, SO_4^{-}• and •OH, so Fukui index representing electrophilic and (f^-) radical attack (f^0) are considered [58].

In this study, CTC was selected to precisely investigate the degradation pathway by means of theoretical calculations, while the degradation intermediates and possible pathways of OTC and TTC are discussed in the ESI and shown in Fig. S9 and Fig. S10, respectively. Fig. 6a shows the molecular structure of CTC after geometrical optimization by Gaussian software, and Fig. 6b presents the calculated Fukui index on electrophilic and (f^-) radical attack (f^0). Generally, the active sites obtained from Fukui index results are consistent with that of the highest occupied molecular orbital (HOMO) distribution of CTC (Fig. 6c). HOMOs indicate the regions which can easily lose electrons for

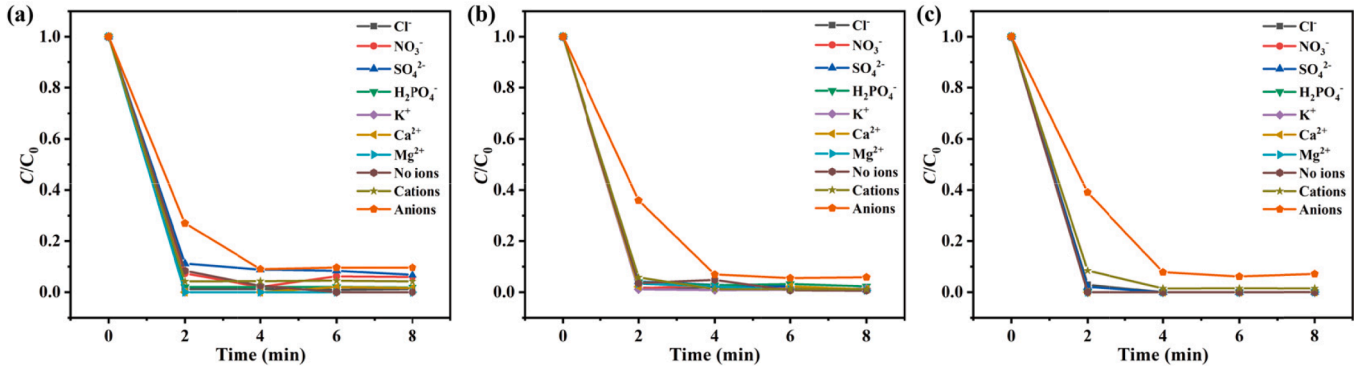

Fig. 4. Effect of co-existing ions on the tetracycline antibiotics matrix degradation of (a) OTC, (b) TTC, (c) CTC over MC. Reaction conditions: MC = 2 g/L, OTC = 10 mg/L, TTC = 10 mg/L, CTC = 10 mg/L, volume = 50 mL, PDS = 1 mM, pH = 4.04 (unadjusted), sampling interval = 2 min, Cl^- = 135.3 mg/L, NO_3^- = 13.6 mg/L, SO_4^{2-} = 124.0 mg/L, $H_2PO_4^-$ = 5 mg/L, K^+ = 4.68 mg/L, Ca^{2+} = 185 mg/L, Mg^{2+} = 39.7 mg/L.

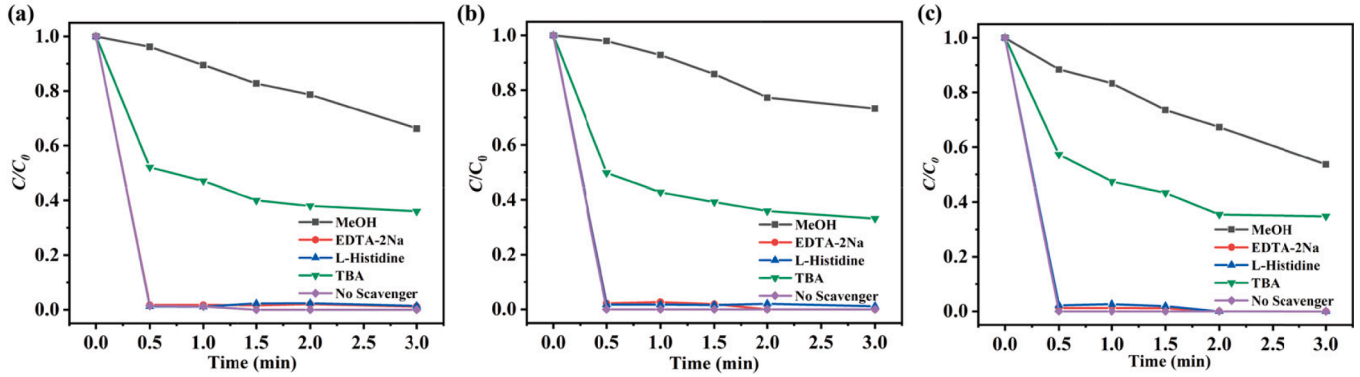

Fig. 5. (a) Effects of different scavengers on (a) OTC, (b) TTC and (c) CTC degradation in the presence of MC, all three tetracycline antibiotics were conducted individually. Reaction conditions: MC = 2 g/L, OTC = 10 mg/L, TTC = 10 mg/L, CTC = 10 mg/L, volume = 50 mL, PDS = 1 mM, pH = 4.04 (unadjusted), sampling interval = 0.5 min.

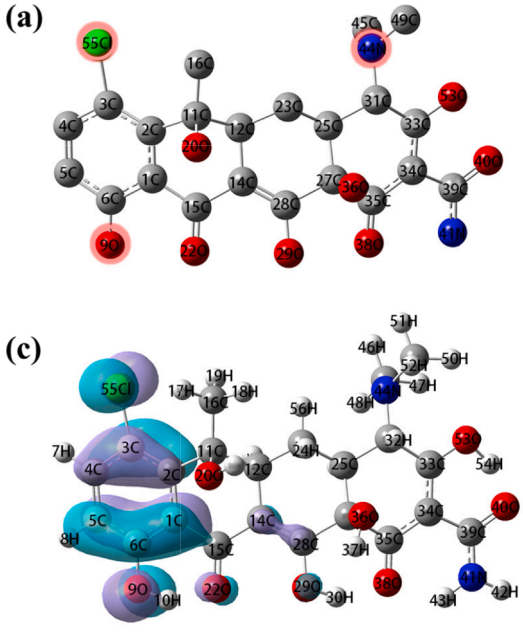

(b)

Atom	No	Charge (0)(e/Å^3)	Charge (+1)(e/Å^3)	Charge (-1)(e/Å^3)	f^-	f^0
C	1	-0.1863	-0.1244	-0.1717	0.0618	0.0236
C	2	-0.0246	-0.0127	-0.0505	0.0119	0.0189
C	3	-0.0589	0.0151	-0.0586	0.0740	0.0369
C	4	-0.2128	-0.2048	-0.2586	0.0080	0.0269
C	5	-0.2760	-0.2290	-0.2955	0.0470	0.0333
C	6	0.3921	0.4289	0.3719	0.0369	0.0285
O	9	-0.6906	-0.5875	-0.7175	0.1031	0.0650
C	11	0.2959	0.2923	0.2983	-0.0036	-0.0030
C	12	-0.2810	-0.2839	-0.2743	-0.0028	-0.0048
C	14	-0.1790	-0.1663	-0.1971	0.0127	0.0154
C	15	0.5477	0.5388	0.4779	-0.0089	0.0305
C	16	-0.7142	-0.7203	-0.7095	-0.0061	-0.0054
O	20	-0.7529	-0.7500	-0.7560	0.0030	0.0030
O	22	-0.5949	-0.5706	-0.6532	0.0243	0.0413
C	23	-0.4681	-0.4696	-0.4641	-0.0015	-0.0028
C	25	-0.2675	-0.2691	-0.2622	-0.0016	-0.0035
C	27	0.1765	0.1738	0.1710	-0.0028	0.0014
C	28	0.3889	0.4227	0.3554	0.0338	0.0337
O	29	-0.6849	-0.6618	-0.7088	0.0231	0.0235
C	31	-0.1128	-0.1231	-0.1025	-0.0103	-0.0103
C	33	0.5322	0.5255	0.4175	-0.0066	0.0540
C	34	-0.3704	-0.3534	-0.3606	0.0169	0.0036
C	35	0.5497	0.5460	0.4455	-0.0037	0.0502
O	36	-0.7504	-0.7432	-0.7759	0.0072	0.0164
O	38	-0.6481	-0.6312	-0.7224	0.0169	0.0456
C	39	0.6900	0.6883	0.6860	-0.0017	0.0011
O	40	-0.6825	-0.6637	-0.7091	0.0189	0.0227
N	41	-0.8193	-0.8073	-0.8370	0.0119	0.0149
N	44	-0.5045	-0.3617	-0.5084	0.1428	0.0733
C	45	-0.4872	-0.5047	-0.4794	-0.0176	-0.0127
C	49	-0.4757	-0.4947	-0.4675	-0.0190	-0.0136
O	53	-0.6563	-0.6495	-0.7177	0.0068	0.0341
Cl	55	-0.0216	0.0860	-0.0571	0.1076	0.0715

Fig. 6. DFT calculations on reactive sites of CTC molecule at the B3LYP/6–31+G(d, p) level. (a) Chemical structure of CTC (red circles indicate the reactive sites); (b) Natural population analysis (NPA) charge populations and condensed Fukui index distribution for electrophilic attack (f^-) and radical attack (f^0); and (c) HOMO distribution of CTC.

electrophilic attack, so for CTC, the atoms in benzene ring associated with –Cl and –OH are more reactive. However, HOMO cannot quantitively describe the reactivity of different sites, and thus, Fukui index is introduced. It can be observed that the Cl44 (f^-/f^0 = 0.1076/0.0715), N44 (f^-/f^0 = 0.1428/0.0733) and O9 (f^-/f^0 = 0.1031/0.0650) exhibit higher Fukui index, which are likely to be attacked by electrophilic $SO_4^{\cdot-}$ and •OH. Fig. 7 displays the degradation pathway of CTC, in which three major pathways are proposed. First, CTC can be transformed to P1 (m/z = 450) *via* demethylation upon the attack of $SO_4^{\cdot-}$ towards N44 atom [59]. Meanwhile, the $SO_4^{\cdot-}$ radicals are likely to attack the acylamino group of CTC (C39, O40 and N31), leading to formation of P2 (m/z = 378). The ring-opening products, including P3 (m/z = 302) and P4 (m/z = 250) are assigned as further degradation intermediates of P2 by both attack of •OH and $SO_4^{\cdot-}$ [60,61].

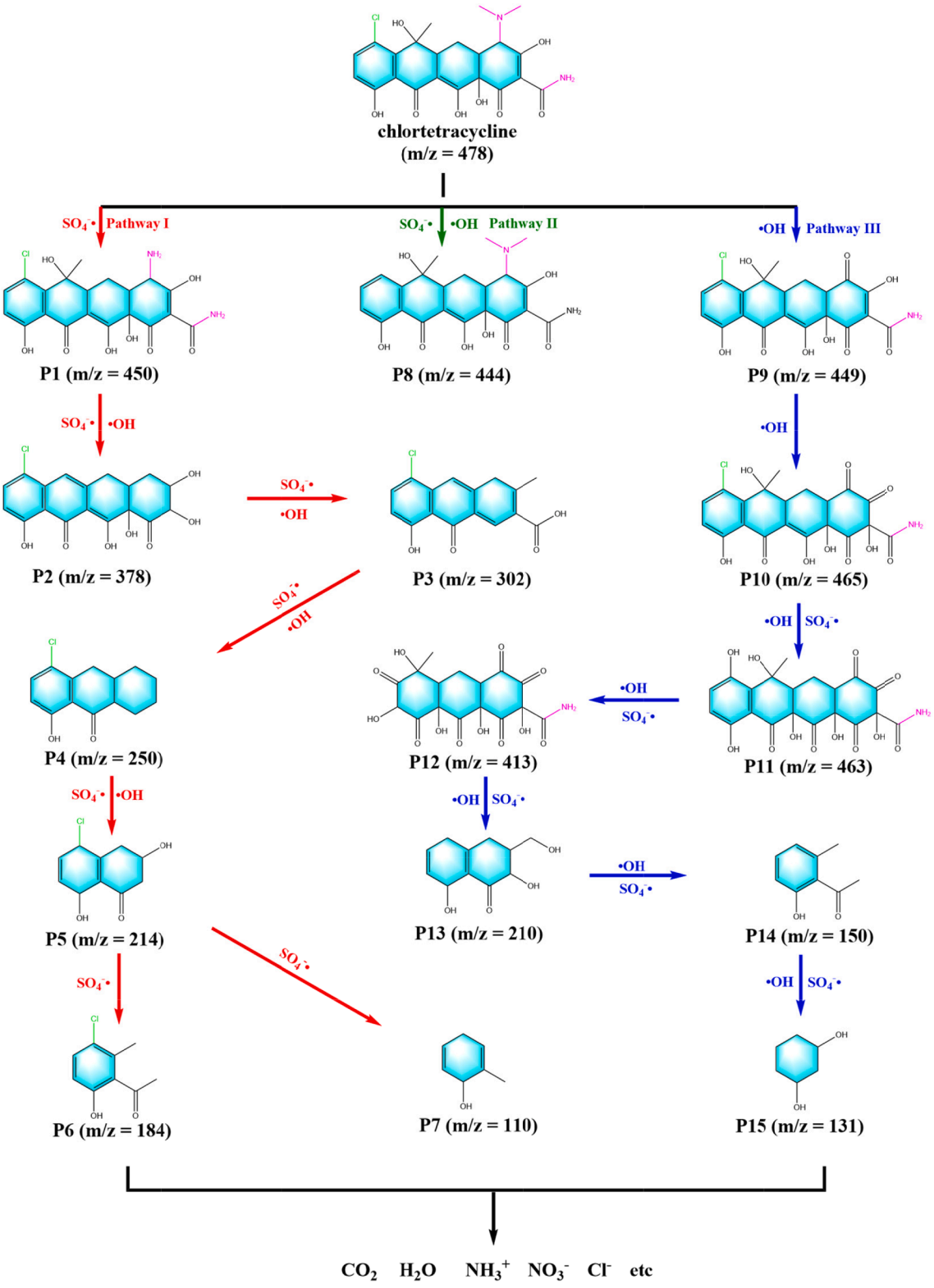

Fig. 7. Proposed CTC degradation pathways by photoactivated SR-AO process over MC.

Meanwhile, P5 (m/z = 214) intermediate is generated due to the cleavage of C=C bond, along with the ring-opening process caused by •OH and SO_4^{-}•. Furthermore, products with smaller molecules, such as P6 (m/z = 184) and P7 (m/z = 110) originate from P5 through a ring-opening step upon the attack of SO_4^{-}• [62]. Notably, the dechloridation on Cl44 atom occurs during the generation of P7, which is similar to "Pathway II" and matches perfectly with the DFT calculation. Secondly, P8 (m/z = 449) is likely to be generated according to a previous report [63] by the dechloridation on Cl44 atom *via* attack of SO_4^{-}• and •OH radicals. As shown in "pathway III", the tertiary amine moiety on the chlortetracycline is attacked by the •OH to form P9 (m/z = 449). Meanwhile, •OH attack on C33 atom results in a keto group substitution, which causes the formation of intermediate P10 (m/z = 465). Then, P10 is converted to P11 (m/z = 463) through the dechloridation and hydroxyl substitution reactions. P12 (m/z = 413), P13 (m/z = 210) and P14 (m/z = 150) are obtained through ring-opening process of P11 [64,65]. More importantly, C=C bond is cleaved in P14 (m/z = 150). P15 (m/z = 131) with smaller molecular weight is formed as a result of the attack by SO_4^{-}• and •OH [66]. As the reaction proceeds, most of the intermediates can be degraded into smaller organic compounds and finally mineralize into CO_2 and H_2O.

The degradation of the selected pollutants can prove the remarkable efficiency of the SR-AOP, and the toxicity of corresponding intermediates may prove this as well [67]. Toxicity Estimation Software (T.E.S.T.), based on quantitative structure–activity relationship (QSAR) prediction, was applied to explore the acute toxicity (Daphnia Magna LC_{50} and Oral Rat LD_{50}), bioaccumulation factor and mutagenicity of three tetracycline antibiotics and their degradation intermediates. The toxicity, bioaccumulation factor, and mutagenicity of CTC (Fig. 8a-c) are discussed in ESI.

The acute toxicity of TTC on the Daphnia Magna LC_{50} is 12.7 mg/L (Fig. 8d), which can be categorized as "harmful" [67]. Nearly all the degradation intermediates of TTC show high LC_{50}, except for P7, indicating the decreased toxicity of the intermediates, especially for P15. Fig. 8e and f reveal that the photoactivated SR-AOP significantly decreases the bioaccumulation factor and mutagenicity of the intermediates compared to the original TTC. For instance, the bioaccumulation factors are decreased by 92% and 93% for intermediates P12 and P13, respectively, compared with that for TTC. TTC is positively mutagenic [68,69] and the SR-AOP changes the mutagenicity of the intermediates to "negative mutagenicity" except for P1, P2, P3, and P6 (Fig. 8f).

As shown in Fig. 8g, the LD_{50} of OTC for rats by oral ingestion is 757.73 mg/kg, which is considered to be "very toxic" [70]. Most of the degradation intermediates of OTC shows higher LD_{50}, indicating that the photoactivated SR-AOP alleviates the oral rat toxicity. However, the degradation intermediates, except for P4 and P11 (for which the LD_{50} values are much higher than that of OTC), are still considered to be toxic. Fig. 8h reveals that the oxidation process also significantly decreases the mutagenicity of OTC. Specifically, OTC is positively mutagenic, while the mutagenicity of all degradation intermediates is lower than that of OTC, while P5, P6, P9, P10, and P13 exhibit negative mutagenicity (Fig. 8i). Therefore, although complete removal of OTC can be obtained within 10 min, the degradation time should be extended

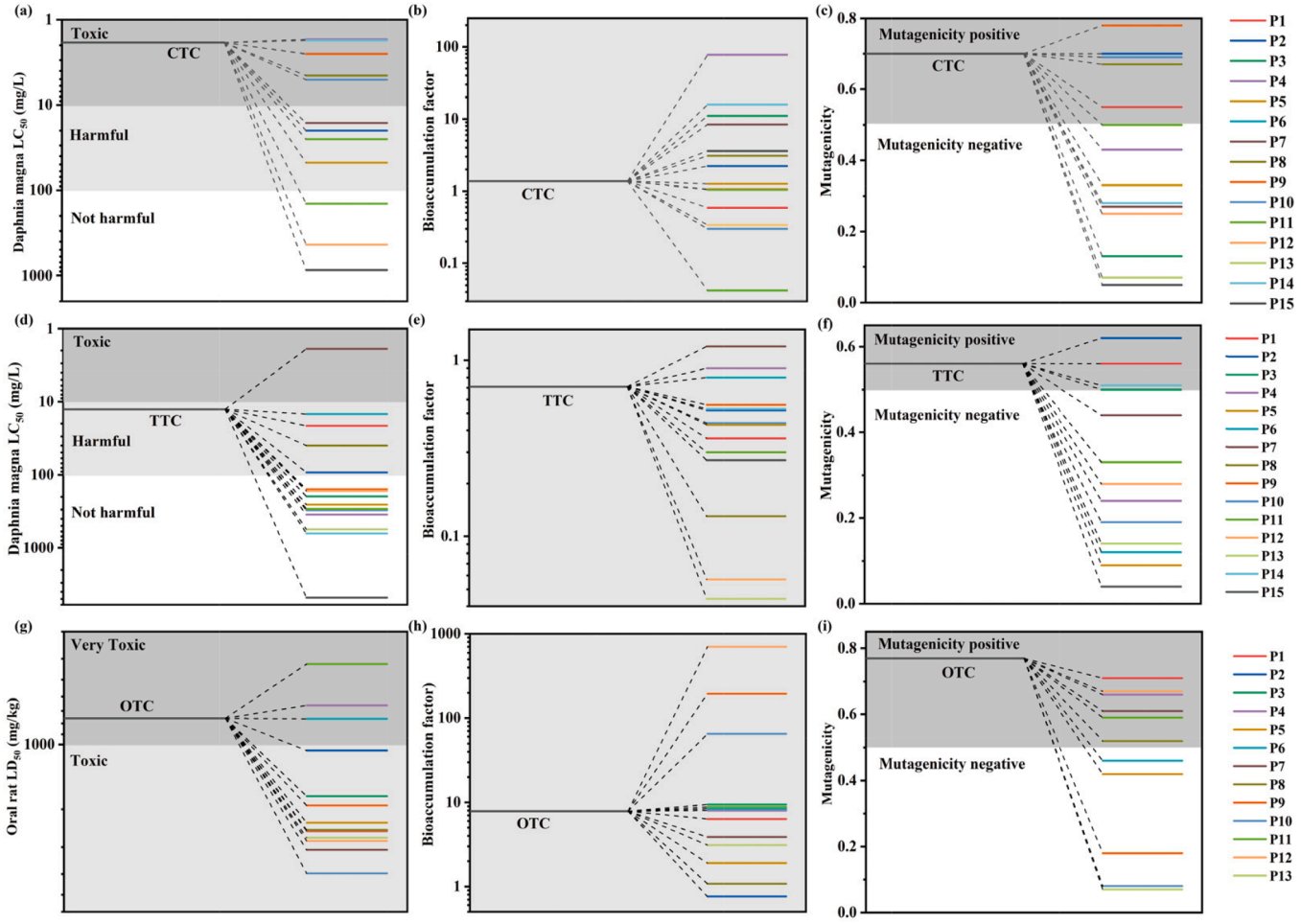

Fig. 8. (a) Daphnia magna LC_{50}, (b) bioaccumulation factor, and (c) mutagenicity of CTC. (d) Daphnia magna LC_{50}, (e) bioaccumulation factor, and (f) mutagenicity of TTC. (g) Oral Rat LD_{50}, (h) bioaccumulation factor, and (i) mutagenicity of OTC and their degradation intermediates.

to achieve better mineralization. The toxicity estimation of OTC in this study suggests that a higher extent of oxidation or mineralization is required to guarantee good water safety after treatment.

Further, we also investigated the existence of intermediates and their toxicity in the final samples collected at 8 min. Taking CTC as example, the HPLC-MS results reveal that CTC degradation intermediates with low molecular weights, such as P7 ($m/z = 110$), P14 ($m/z = 150$) and P15 ($m/z = 131$) are detected in the sample collected at 8 min. The LC_{50}, bioaccumulation factor, and mutagenicity of the above-mentioned intermediates are lower than those of CTC. These results imply that high mineralization and detoxification can occur to CTC during SR-AOP. In all, the above results show that photoactivated SR-AOP over MC cannot only accomplish the complete removal of tetracycline antibiotics matrix, but also the decreases the toxicity of OTC, TTC, and CTC.

3.2.6. Reusability and stability of MC in batch experiments

Powder-based catalysts typically suffer from difficult recovery and poor recyclability in wastewater treatment, which hinder their practical applications [71]. Our strategy of immobilizing MIL-88A(Fe) particles on cotton fibers leads to both easy recyclability and long-term operation for the removal of inorganic and organic arsenic pollutants [29]. In this work, MC is suspended in aqueous solutions containing OTC, TTC, and CTC matrix to test the recyclability, stability, and performance for long-term photoactivated SR-AOP in the presence of UV-LED light and PDS (Fig. 9). The results show that high degradation efficiencies (from 98.2%, 98.3%, and 100% to 83.7%, 78.8, and 88.1% for OTC, TTC, and CTC, respectively) towards OTC, TTC and CTC can be achieved over MC after 30 cycles of consecutive run in 240 min, thus affirming the long-term catalytic performance of MC. By comparing the SEM images, FTIR spectra, XPS spectra, and PXRD patterns of MC before and after photoactivated SR-AOP (Fig. 10 and Fig. S11-13), it is found that the original morphology and structure of MC are successfully maintained after 30 cycles, indicating the good stability and reusability of MC. To further confirm the stability of MC, the leaching of Fe ions in treated solutions were determined by ICP-OES. As shown in Fig. S14, the leached iron is lower than 3.0 mg/L after 8 cycles and decreases to 0.22 mg/L in subsequent cycles, demonstrating that the immobilized MIL-88A(Fe) is stably anchored to the cotton fibers.

To further highlight the advantages of MC, the photoactivated SR-AOP performance of MIL-88A powder was compared with that of MC under identical conditions. The results show that after the reaction, the aqueous solution treated using MIL-88A powder is turbid due to the suspended MIL-88A, while the solution treated by MC is clear and free of suspended MIL-88A particles (Fig. S15).

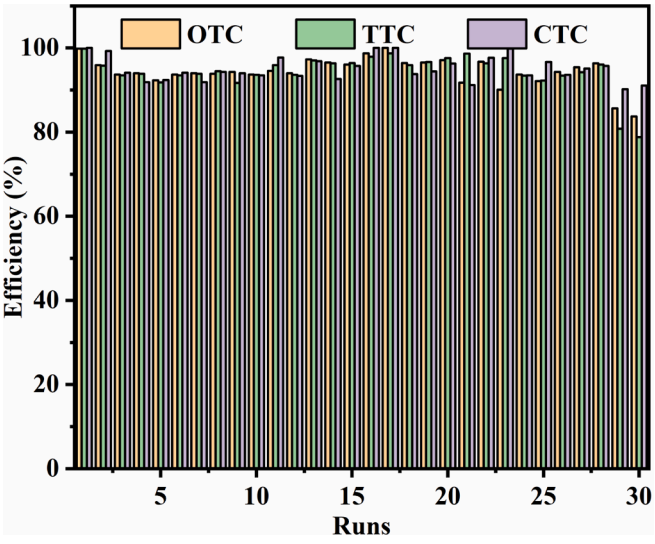

Fig. 9. Removal efficiencies of tetracycline antibiotics matrix over MC in 30 consecutive runs under UV light in batch experiment. Reaction conditions: MC = 2 g/L, OTC = 10 mg/L, TTC = 10 mg/L, CTC = 10 mg/L, volume = 50 mL, PDS = 1 mM, pH = 4.04, 5 W UV-LED light irradiation (Beijing Perfectlight Co., Ltd., PCX-50B, wavelength at 369 nm).

3.3. Degradation of tetracycline antibiotics matrix in a fixed bed reactor

The special structure of cotton fiber makes it an ideal material to pack a fixed bed reactor due to its good flexibility. From our recyclability experiment (Fig. 9), the as-prepared MC can be used as an effective and long-term catalyst in photoactivated SR-AOP. To test the possible continuous operation of the photoactivated SR-AOP over MC catalyst, a fixed bed reactor was constructed by packing MC in the annular channel of a self-designed quartz equipment. In order to maintain the amount of substance and ratio of different solutions in fixed bed reactor and batch experiment, the flow rate of the aqueous solution containing tetracycline antibiotics matrix and PDS solution was calculated based on the results of the batch experiments following Eq. (5) [72], where Q_{TCs} and Q_{PDS} are the flow rate of tetracycline antibiotics matrix solution and PDS solution, V_{TCs} and V_{PDS} are volume of tetracycline antibiotics matrix solution and PDS solution in batch experiment, respectively. The hydraulic retention time (HRT) is calculated to be 10 min (Eq. (6)), according to the degradation performance in batch experiments, in which V is the effective volume of the fixed bed reactor. Therefore, the flow rate of tetracycline antibiotics matrix solution and PDS solution was set at 0.2 L/h and 3.0 mL/h, respectively. As shown in Fig. 11, complete removal of all three tetracycline antibiotics can be achieved within 22 h. A slight drop in catalytic degradation efficiency is observed from 23 to 24 h, in which 80% of OTC and TTC, and 90% of CTC are successfully removed from the simulated wastewater. The SEM image in Fig. S16 suggests that the immobilized MIL-88A can maintain its structure and morphology, implying its potential utilization for practical wastewater treatment. It is worth noting that 4.8 L of simulated wastewater containing three tetracycline antibiotics matrix can be completely purified by the photoactivated SR-AOP system using 6.204 g of MC (0.204 g MIL-88A(Fe) as effective dosage) catalyst. It can be calculated that 1.0 kg MIL-88A(Fe) catalyst in MC can accomplish complete purification towards 23.5 t of wastewater containing OTC, TTC, and CTC, each with initial concentration of 10 mg/L within 24 h. It is speculated that the static MC in the fixed bed reactor can partly overcome the hydrodynamic shear stress from the influent, which can further protect MIL-88A from the attack of water molecules. In all, our approach of packing MC catalyst in a fixed bed reactor provides a positive feedback towards the long-term application of MIL-88A in photoactivated SR-AOP, which inspires us to explore large-scale water purification with the aid of MOFs, (*e.g.*, MIL-88A) as catalysts.

$$Q_{TCs}/Q_{PDS} = V_{TCs}/V_{PDS} \quad (5)$$

$$HRT = V/Q_{TCs} \quad (6)$$

4. Conclusions

This work has demonstrated the eco-friendly production and application of MC for PDS activation under UV-light irradiation. The characterization results, including PXRD, UV–vis DRS, XPS, FTIR and SEM confirm the successful immobilization of MIL-88A(Fe) on cotton fibers. Additionally, the XPS analysis shows the appearance of Fe-O bond which proves the successful linkage of MIL-88A(Fe) to cotton fibers. The as-prepared MC is highly effective for the degradation of tetracycline antibiotics matrix and the fixed bed reactor constructed based on MC exhibits a remarkable ability for the continuous removal of simulated wastewater containing tetracycline antibiotics matrix, with little effect from initial pH value and inorganic ions. The superior stability/reusability of MC is confirmed by 30 cycles of consecutive runs, in which the

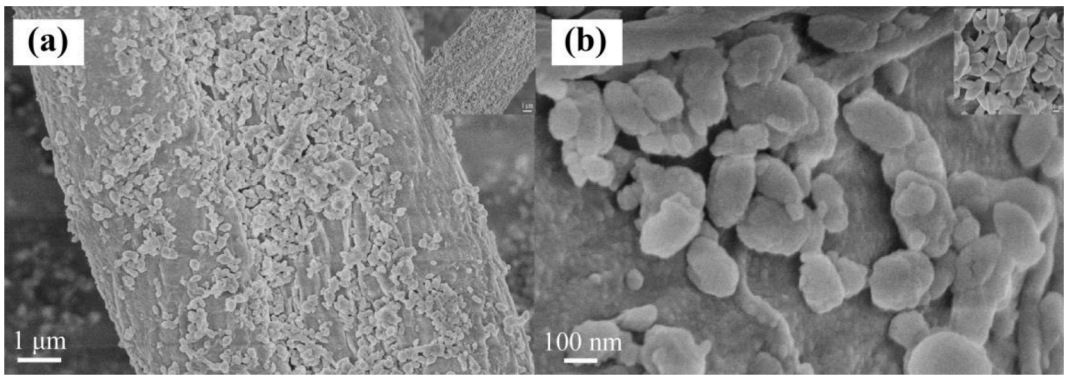

Fig. 10. (a) and (b) SEM images of MC after 30 cycles of batch experiment. The insets show the SEM images of MC before 30 cycles of batch experiment.

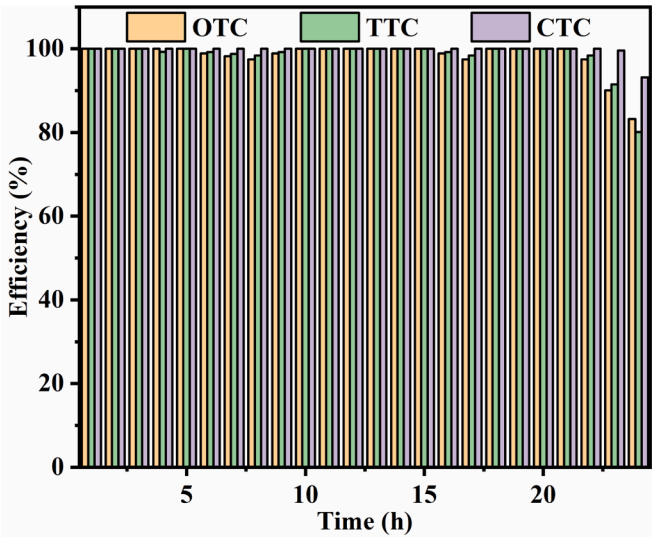

Fig. 11. Removal efficiencies of tetracycline antibiotics matrix over MC in fixed bed reactor. Reaction conditions: MC = 6.204 g, OTC = 10 mg/L, TTC = 10 mg/L, CTC = 10 mg/L, 10 W UV-Hg light irradiation (CNLight).

removal efficiency is well-maintained within 8 min for each cycle. The fixed bed experiments further reveal that within 24 h, 4.8 L of tetracycline antibiotics matrix solution can be successfully treated and over 80% of antibiotics can be removed after 24 h, corresponding to 23.5 t of wastewater for every 1 kg of MIL-88A(Fe). The possible mechanism was explored through active species scavenging experiments, revealing that SO_4^{-}• radicals are the primary active species, while •OH is the second main radical in the reaction system. LC-MS analysis and DFT calculations were conducted to explore the possible degradation pathways of OTC, TTC, and CTC. The toxicity of OTC, TTC, CTC and degradation intermediates were assessed as well, showing that photoactivated SR-AOP over MC leads to both complete removal of tetracycline antibiotics matrix and decreased toxicity of OTC, TTC, and CTC. These results confirm the promising potential of MOFs as effective catalysts for continuous removal of pollutants from wastewater.

CRediT authorship contribution statement

Jia-Sheng Wang: Data curation, Investigation, Visualization, Writing – original draft. **Xiao-Hong Yi:** Validation, Methodology. **Xingtao Xu:** Validation, Writing – review & editing. **Haodong Ji:** Software, Methodology. **Amer M. Alanazi:** Validation, Writing – review & editing. **Chong-Chen Wang:** Conceptualization, Funding acquisition, Supervision, Project administration, Writing – review & editing. **Chen Zhao:** Software, Methodology. **Yusuf Valentino Kaneti:** Validation, Writing – review & editing. **Peng Wang:** Resources. **Wen Liu:** Validation, Software, Writing – review & editing. **Yusuke Yamauchi:** Validation, Writing – review & editing.

Declaration of Competing Interest

The authors declare that they have no known competing financial interests or personal relationships that could have appeared to influence the work reported in this paper.

Acknowledgments

This work was supported by National Natural Science Foundation of China (22176012, 21806008), Beijing Natural Science Foundation (8202016), Great Wall Scholars Training Program Project of Beijing Municipality Universities (CIT&TCD20180323), Beijing Talent Project (2020A27), Science and Technology General Project of Beijing Municipal Education Commission (KM202110016010), JST-ERATO Yamauchi Materials Space-Tectonics Project (JPMJER2003), The Fundamental Research Funds for Beijing University of Civil Engineering and Architecture (X20147, X20141, X20135, X20146), and the Researchers Supporting Project Number (RSP-2021/261) King Saud University, Riyadh, Saudi Arabia. This work was performed in part at the Queensland node of the Australian National Fabrication Facility, a company established under the National Collaborative Research Infrastructure Strategy to provide nano and microfabrication facilities for Australia's researchers.

Appendix A. Supplementary data

Supplementary data to this article can be found online at https://doi.org/10.1016/j.cej.2021.133213.

References

[1] Z. Yang, X. Xia, L. Shao, L. wang, Y. Liu, Efficient photocatalytic degradation of tetracycline under visible light by Z-scheme Ag_3PO_4/mixed-valence MIL-88A(Fe) heterojunctions: Mechanism insight, degradation pathways and DFT calculation, Chem. Eng. J. 410 (2021), 128454.
[2] B. Li, T. Zhang, Mass flows and removal of antibiotics in two municipal wastewater treatment plants, Chemosphere 83 (2011) 1284–1289.
[3] X.-S. Miao, F. Bishay, M. Chen, C.D. Metcalfe, Occurrence of antimicrobials in the final effluents of wastewater treatment plants in Canada, Environ. Sci. Technol. 38 (2004) 3533–3541.
[4] Q. Qiu, G. Li, Y. Dai, Y. Xu, P. Bao, Removal of antibiotic resistant microbes by Fe (II)-activated persulfate oxidation, J. Hazard. Mater. 396 (2020), 122733.
[5] A.K. Sarmah, M.T. Meyer, A.B.A. Boxall, A global perspective on the use, sales, exposure pathways, occurrence, fate and effects of veterinary antibiotics (VAs) in the environment, Chemosphere 65 (2006) 725–759.
[6] Q. Zhu, Y. Sun, F. Na, J. Wei, S. Xu, Y. Li, F. Guo, Fabrication of CdS/titanium-oxo-cluster nanocomposites based on a Ti_{32} framework with enhanced photocatalytic activity for tetracycline hydrochloride degradation under visible light, Appl. Catal. B 254 (2019) 541–550.
[7] W. Dai, L. Jiang, J. Wang, Y. Pu, Y. Zhu, Y. Wang, B. Xiao, Efficient and stable photocatalytic degradation of tetracycline wastewater by 3D polyaniline/perylene

diimide organic heterojunction under visible light irradiation, Chem. Eng. J. 397 (2020), 125476.
[8] J. Lu, Y. Zhang, J. Wu, J. Wang, Y. Cai, Fate of antibiotic resistance genes in reclaimed water reuse system with integrated membrane process, J. Hazard. Mater. 382 (2020), 121025.
[9] S. Zhang, Y.-L. Yang, J. Lu, X.-J. Zuo, X.-L. Yang, H.-L. Song, A review of bioelectrochemical systems for antibiotic removal: Efficient antibiotic removal and dissemination of antibiotic resistance genes, J. Water Process. 37 (2020), 101421.
[10] W. Ren, G. Nie, P. Zhou, H. Zhang, X. Duan, S. Wang, The intrinsic nature of persulfate activation and N-doping in carbocatalysis, Environ. Sci. Technol. 54 (2020) 6438–6447.
[11] Q. Ke, Y. Shi, Y. Liu, F. Chen, H. Wang, X.-L. Wu, H. Lin, J. Chen, Enhanced catalytic degradation of bisphenol A by hemin-MOFs supported on boron nitride via the photo-assisted heterogeneous activation of persulfate, Sep. Purif. Technol. 229 (2019), 115822.
[12] S. Wacławek, H.V. Lutze, K. Grübel, V.V.T. Padil, M. Černík, D.D. Dionysiou, Chemistry of persulfates in water and wastewater treatment: A review, Chem. Eng. J. 330 (2017) 44–62.
[13] W. Shang, Z. Dong, M. Li, X. Song, M. Zhang, C. Jiang, S. Feiyun, Degradation of diatrizoate in water by Fe(II)-activated persulfate oxidation, Chem. Eng. J. 361 (2019) 1333–1344.
[14] X. Duan, H. Sun, S. Wang, Metal-Free Carbocatalysis in Advanced Oxidation Reactions, Acc. Chem. Res. 51 (2018) 678–687.
[15] J. Li, Y. Wan, Y. Li, G. Yao, B. Lai, Surface Fe(III)/Fe(II) cycle promoted the degradation of atrazine by peroxymonosulfate activation in the presence of hydroxylamine, Appl. Catal. B 256 (2019), 117782.
[16] H. Zheng, J. Bao, Y. Huang, L. Xiang, B. Faheem, J. Ren, M.N. Du, D.D. D. Nadagouda, Efficient degradation of atrazine with porous sulfurized Fe_2O_3 as catalyst for peroxymonosulfate activation, Appl. Catal. B 259 (2019), 118056.
[17] J. Jin, Z. Yang, W. Xiong, Y. Zhou, R. Xu, Y. Zhang, J. Cao, X. Li, C. Zhou, Cu and Co nanoparticles co-doped MIL-101 as a novel adsorbent for efficient removal of tetracycline from aqueous solutions, Sci. Total Environ. 650 (2019) 408–418.
[18] Y. Zhang, J. Zhou, J. Chen, X. Feng, W. Cai, Rapid degradation of tetracycline hydrochloride by heterogeneous photocatalysis coupling persulfate oxidation with MIL-53(Fe) under visible light irradiation, J. Hazard. Mater. 392 (2020), 122315.
[19] Y. Ren, T. Li, W. Zhang, S. Wang, M. Shi, C. Shan, W. Zhang, X. Guan, L. Lv, M. Hua, B. Pan, MIL-PVDF blend ultrafiltration membranes with ultrahigh MOF loading for simultaneous adsorption and catalytic oxidation of methylene blue, J. Hazard. Mater. 365 (2019) 312–321.
[20] S. Zheng, X. Li, B. Yan, Q. Hu, Y. Xu, X. Xiao, H. Xue, H. Pang, Transition-metal (Fe Co, Ni) based metal-organic frameworks for electrochemical energy storage, Adv. Energy Mater. 7 (2017) 1602733.
[21] K. Laurier, F. Vermoortele, R. Ameloot, D. De Vos, J. Hofkens, M. Roeffaers, Iron (III)-based metal–organic frameworks as visible light photocatalysts, J. Am. Chem. Soc. 135 (39) (2013) 14488–14491.
[22] D. Wang, M. Wang, Z. Li, Fe-based metal-organic frameworks for highly selective photocatalytic benzene hydroxylation to phenol, ACS Catal. 5 (11) (2015) 6852–6857.
[23] J. Tang, J. Wang, Metal organic framework with coordinatively unsaturated sites as efficient Fenton-like catalyst for enhanced degradation of sulfamethazine, Environ. Sci. Technol. 52 (9) (2018) 5367–5377.
[24] X.H. Yi, C.C. Wang, Elimination of emerging organic contaminants in wastewater by advanced oxidation process over iron-based MOFs and their composites, Prog. Chem. 33 (2021) 471–489.
[25] M. Wen, G. Li, H. Liu, J. Chen, T. An, H. Yamashita, Metal–organic framework-based nanomaterials for adsorption and photocatalytic degradation of gaseous pollutants: recent progress and challenges, Environ. Sci: Nano 6 (4) (2019) 1006–1025.
[26] Y. Zhang, J. Zhou, X. Chen, L. Wang, W. Cai, Coupling of heterogeneous advanced oxidation processes and photocatalysis in efficient degradation of tetracycline hydrochloride by Fe-based MOFs: Synergistic effect and degradation pathway, Chem. Eng. J. 369 (2019) 745–757.
[27] H. Hu, H. Zhang, Y. Chen, Y. Chen, L. Zhuang, H. Ou, Enhanced photocatalysis degradation of organophosphorus flame retardant using MIL-101(Fe)/persulfate: Effect of irradiation wavelength and real water matrixes, Chem. Eng. J. 368 (2019) 273–284.
[28] W.-T. Xu, L. Ma, F. Ke, F.-M. Peng, G.-S. Xu, Y.-H. Shen, J.-F. Zhu, L.-G. Qiu, Y.-P. Yuan, Metal–organic frameworks MIL-88A hexagonal microrods as a new photocatalyst for efficient decolorization of methylene blue dye, Dalton Trans. 43 (2014) 3792–3798.
[29] D. Pang, C.-C. Wang, P. Wang, W. Liu, H. Fu, C. Zhao, Superior removal of inorganic and organic arsenic pollutants from water with MIL-88A(Fe) decorated on cotton fibers, Chemosphere 254 (2020) 126829.
[30] J. Wang, J. Wan, Y. Ma, Y. Wang, M. Pu, Z. Guan, Metal–organic frameworks MIL-88A with suitable synthesis conditions and optimal dosage for effective catalytic degradation of Orange G through persulfate activation, RSC Adv. 6 (2016) 112502–112511.
[31] B. Xla, W.A. Fan, W.C. Fang, C.A. Yi, Y. Yue, C. Btt, B. Qha, B. Sla, Synthesis of (100) surface oriented MIL-88A-Fe with rod-like structure and its enhanced fenton-like performance for phenol removal, Appl. Catal. B 259 (2019) 118064.
[32] X.-H. Yi, H. Ji, C.-C. Wang, Y. Li, Y.-H. Li, C. Zhao, A. Wang, H. Fu, P. Wang, X. Zhao, W. Liu, Photocatalysis-activated SR-AOP over PDINH/MIL-88A(Fe) composites for boosted chloroquine phosphate degradation: performance, mechanism, pathway and DFT calculations, Appl. Catal. B 293 (2021), 120229.
[33] H. Fu, X.-X. Song, L. Wu, C. Zhao, P. Wang, C.-C. Wang, Room-temperature preparation of MIL-88A as a heterogeneous photo-Fenton catalyst for degradation of rhodamine B and bisphenol a under visible light, Mater. Res. Bull. 125 (2020), 110806.
[34] M. Yadav, S. Garg, A. Chandra, K. Hernadi, Immobilization of green BiOX (X= Cl, Br and I) photocatalysts on ceramic fibers for enhanced photocatalytic degradation of recalcitrant organic pollutants and efficient regeneration process, Ceram. Int. 45 (2019) 17715–17722.
[35] X. Liao, F. Wang, F. Wang, Y. Cai, Y. Yao, B.-T. Teng, Q. Hao, L. Shuxiang, Synthesis of (100) surface oriented MIL-88A-Fe with rod-like structure and its enhanced fenton-like performance for phenol removal, Appl. Catal. B 259 (2019), 118064.
[36] J. Amaro-Gahete, R. Klee, D. Esquivel, José.R. Ruiz, César Jiménez-Sanchidrián, F. José. Romero-Salguero, Fast ultrasound-assisted synthesis of highly crystalline MIL-88A particles and their application as ethylene adsorbents, Ultrason. Sonochem. 50 (2019) 59–66.
[37] T. Chalati, P. Horcajada, R. Gref, P. Couvreur, C. Serre, Optimisation of the synthesis of MOF nanoparticles made of flexible porous iron fumarate MIL-88A, J. Mater. Chem. 21 (7) (2011) 2220–2227.
[38] J. Tisheng, Q. Junyu, W. Mingyu, L. Qingzhe, Q. Cixiao, C. Junyao, Seasonal variations of hydrochemical characteristics of groundwater in Changping Plain, Beijing, J. Res. Ecol. 8 (2017) 655–663.
[39] A. Liu, C.-C. Wang, C.-zheng. Wang, H.-fen. Fu, W. Peng, Y.-L. Cao, H.-Y. Chu, A.-F. Du, Selective adsorption activities toward organic dyes and antibacterial performance of silver-based coordination polymers, J. Colloid Interface Sci. 512 (2018) 730–739.
[40] D. Chen, X. Yi, L. Ling, C. Wang, P. Wang, Photocatalytic Cr(VI) sequestration and photo-Fenton bisphenol A decomposition over white light responsive PANI/MIL-88A(Fe), Appl. Organomet. Chem. 34 (2020).
[41] S. Jiao, S. Zheng, D. Yin, L. Wang, L. Chen, Aqueous oxytetracycline degradation and the toxicity change of degradation compounds in photoirradiation process, J. Environ. Sci. 20 (2008) 806–813.
[42] Z. Li, P.H. Chang, J.S. Jean, W.T. Jiang, C.J. Wang, Interaction between tetracycline and smectite in aqueous solution, J. Colloid Interface Sci. 341 (2010) 311–319.
[43] G. Lü, L. Wu, X. Wang, L. Liao, X. Wang, Adsorption of chlortetracycline from water by rectories, Chin. J. Chem. Eng. 20 (2012) 1003–1007.
[44] M.B. Ahmed, J.L. Zhou, H.H. Ngo, W. Guo, Adsorptive removal of antibiotics from water and wastewater: progress and challenges, Sci. Total Environ. 532 (2015).
[45] D. Wang, F. Jia, H. Wang, F. Chen, Y. Fang, W. Dong, G. Zeng, X. Li, Q. Yang, X. Yuan, Simultaneously efficient adsorption and photocatalytic degradation of tetracycline by Fe-based MOFs, J. Colloid Interface Sci. 519 (2018) 273–284.
[46] Z. Zhang, Y. Chen, Z. Wang, C. Hu, D. Ma, W. Chen, T. Ao, Effective and structure-controlled adsorption of tetracycline hydrochloride from aqueous solution by using Fe-based metal-organic frameworks, Appl. Surf. Sci. 542 (2021), 148662.
[47] P. Kumar, B. Anand, Y.F. Tsang, K.-H. Kim, S. Khullar, B. Wang, Regeneration, degradation, and toxicity effect of MOFs: Opportunities and challenges, Environ. Res. 176 (2019), 108488.
[48] S. Yuan, L. Feng, K. Wang, J. Pang, M. Bosch, C. Lollar, Y. Sun, J. Qin, X. Yang, P. Zhang, Q. Wang, L. Zou, Y. Zhang, L. Zhang, Y. Fang, J. Li, H.-C. Zhou, Stable metal-organic frameworks: Design, synthesis, and applications, Adv. Mater. 30 (2018) 1704303.
[49] M. Pu, Y. Ma, J. Wan, Y. Wang, J. Wang, M.L. Brusseau, Activation performance and mechanism of a novel heterogeneous persulfate catalyst: Metal organic framework MIL-53(Fe) with Fe(II)/Fe(III) mixed-valence coordinative unsaturated iron center, Catal. Sci. Technol. 7 (2017) 1129–1140.
[50] G.J. Palm, T. Lederer, P. Orth, W. Saenger, M. Takahashi, W. Hillen, W. Hinrichs, Specific binding of divalent metal ions to tetracycline and to the Tet repressor/tetracycline complex, J. Biol. Inorg. Chem. 13 (2008) 1097–1110.
[51] J. Lee, U. von Gunten, J.H. Kim, Persulfate-based advanced oxidation: Critical assessment of opportunities and roadblocks, Environ. Sci. Technol. 54 (2020) 3064–3081.
[52] C. Zhao, J. Wang, X. Chen, Z. Wang, H. Ji, L. Chen, W. Liu, C.C. Wang, Bifunctional $Bi_{12}O_{17}Cl_2$/MIL-100(Fe) composites toward photocatalytic Cr(VI) sequestration and activation of persulfate for bisphenol A degradation, Sci. Total Environ. 752 (2021), 141901.
[53] Y. Wang, X. Zhao, D. Cao, Y. Wang, Y. Zhu, Peroxymonosulfate enhanced visible light photocatalytic degradation bisphenol A by single-atom dispersed Ag mesoporous g-C_3N_4 hybrid, Appl. Catal. B 211 (2017) 79–88.
[54] C.-W. Wang, C. Liang, Oxidative degradation of TMAH solution with UV persulfate activation, Chem. Eng. J. 254 (2014) 472–478.
[55] X. Li, W. Guo, Z. Liu, R. Wang, H. Liu, Fe-based MOFs for efficient adsorption and degradation of acid orange 7 in aqueous solution via persulfate activation, Appl. Surf. Sci. 369 (2016) 130–136.
[56] X. Zhang, H. Deng, G. Zhang, F. Yang, G.-E. Yuan, Natural bornite as an efficient and cost-effective persulfate activator for degradation of tetracycline: Performance and mechanism, Chem. Eng. J. 381 (2020), 122717.
[57] P. Sun, H. Liu, M. Feng, L. Guo, Z. Zhai, Y. Fang, X. Zhang, V.K. Sharma, Nitrogen-sulfur co-doped industrial graphene as an efficient peroxymonosulfate activator: Singlet oxygen-dominated catalytic degradation of organic contaminants, Appl. Catal. B 251 (2019) 335–345.
[58] R.G. Parr, W. Yang, Density functional approach to the frontier-electron theory of chemical reactivity, J. Am. Chem. Soc. 106 (1984) 4049–4050.
[59] R. Pulicharla, R. Drouinaud, S.K. Brar, P. Drogui, F. Proulx, M. Verma, R. Y. Surampalli, Activation of persulfate by homogeneous and heterogeneous iron catalyst to degrade chlortetracycline in aqueous solution, Chemosphere 207 (2018) 543–551.

[60] Z. Li, C. Guo, J. Lyu, Z. Hu, M. Ge, Tetracycline degradation by persulfate activated with magnetic Cu/$CuFe_2O_4$ composite: Efficiency, stability, mechanism and degradation pathway, J. Hazard. Mater. 373 (2019) 85–96.
[61] Y. Liu, Y. Gao, B. Yao, D. Zou, Removal of chlortetracycline by nano- micro-electrolysis materials: Application and mechanism, Chemosphere 238 (2020), 124543.
[62] D. Liu, M. Li, X. Li, F. Ren, P. Sun, L. Zhou, Core-shell Zn/Co MOFs derived Co_3O_4/CNTs as an efficient magnetic heterogeneous catalyst for persulfate activation and oxytetracycline degradation, Chem. Eng. J. 387 (2020), 124008.
[63] Y. Tian, J. Zou, L. Feng, L. Zhang, Y. Liu, Chlorella vulgaris enhance the photodegradation of chlortetracycline in aqueous solution via extracellular organic matters (EOMs): Role of triplet state EOMs, Water Res. 149 (2019) 35–41.
[64] Y. Chen, R. Yin, L. Zeng, W. Guo, M. Zhu, Insight into the effects of hydroxyl groups on the rates and pathways of tetracycline antibiotics degradation in the carbon black activated peroxydisulfate oxidation process, J. Hazard. Mater. 412 (2021), 125256.
[65] J. Jeong, W. Song, W.J. Cooper, J. Jung, J. Greaves, Degradation of tetracycline antibiotics: Mechanisms and kinetic studies for advanced oxidation/reduction processes, Chemosphere 78 (2010) 533–540.
[66] M. Zhang, Q. Shi, X. Cheng, J. Yang, Z. Liu, T. Chen, Y. Qu, J. Wang, M. Xie, W. Han, Accelerated generation of hydroxyl radical through surface polarization on $BiVO_4$ microtubes for efficient chlortetracycline degradation, Chem. Eng. J. 400 (2020), 125871.
[67] Z. Cai, X. Hao, X. Sun, P. Du, W. Liu, J. Fu, Highly active WO_3@anatase-SiO_2 aerogel for solar-light-driven phenanthrene degradation: Mechanism insight and toxicity assessment, Water Res. 162 (2019) 369–382.
[68] F. Lunghini, G. Marcou, P. Azam, M.H. Enrici, E. Van Miert, A. Varnek, Consensus QSAR models estimating acute toxicity to aquatic organisms from different trophic levels: algae, Daphnia and fish, SAR QSAR Environ. Res. 31 (9) (2020) 655–675.
[69] N. Kluver, C. Vogs, R. Altenburger, B.I. Escher, S. Scholz, Development of a general baseline toxicity QSAR model for the fish embryo acute toxicity test, Chemosphere 164 (2016) 164–173.
[70] J. Wu, Q. Xiong, J. Liang, Q. He, D. Yang, R. Deng, Y. Chen, Degradation of benzotriazole by DBD plasma and peroxymonosulfate: Mechanism, degradation pathway and potential toxicity, Chem. Eng. J. 384 (2020), 123300.
[71] M.N. Chong, B. Jin, C.W.K. Chow, C. Saint, Recent developments in photocatalytic water treatment technology: a review, Water Res. 44 (10) (2010) 2997–3027.
[72] X. Xu, W. Chen, S. Zong, X. Ren, D. Liu, Magnetic clay as catalyst applied to organics degradation in a combined adsorption and Fenton-like process, Chem. Eng. J. 373 (2019) 140–149.